University of Baghdad
College of Engineering
JE
JOURNAL OF ENGINEERING

Journal of Engineering

journal homepage: www.jcoeng.edu.iq

Volume 30 Number 4 April 2024

Optimization and Simulation Parameters of the Resistance Spot Welding for Commercial Aluminium (AA1050) at Low Power Welding Machine

Safi R. Safi[1,*], Moneer H. Tolephih[2], Muhsin J. Jweeg[3]

[1]Department of Mechanical Engineering, College of Engineering, University of Baghdad, Baghdad, Iraq
[2]University of Baghdad, Baghdad, Iraq
[3]Al-Farahidi University, Baghdad, Iraq
safi.isaac2003m@coeng.uobaghdad.edu.iq[1], monerht@uobaghdad.edu.iq[2],
muhsin.jweeg@uoalfarahidi.edu.iq[3]

ABSTRACT

This study aims to find the best conditions of resistance spot welding in commercial Aluminium AA1050 to obtain the maximum tensile shear strength of the joint using a low-power supply welding machine. The chosen parameters for this study were welding current, welding time, and electrode force using a 90 kVA welding machine. The investigation used the DoE method with Taguchi's technique to reduce the number of experiments where two sheet thicknesses (1 mm and 2 mm) were used in this work. The software program Minitab 18 analyzed the results using the main effects plots and the interaction plots to identify the most significant parameters and their effect on the joint strength. The best conditions for maximum tensile shear force were 14.85 kA welding current and 0.79 kN electrode force for both thicknesses and two cycles and 12 cycles welding time for 1 mm and 2 mm sheet thickness, respectively. The maximum tensile strength obtained was 250 N and 225 N for 1mm and 2mm sheet thickness, respectively. A mathematical equation was developed to predict the shear force with 19.9 % and 17.9 % error for 1 mm and 2 mm thicknesses, respectively. The best conditions were applied in ANSYS 2022R1 multi-physics to obtain the temperature distribution with time history, where the result shows the nugget size according to the molten temperature. The percentage of discrepancy between actual and numerical nugget size was 8 %.

Keywords: Resistance spot welding, Commercial Aluminium AA1050, Taguchi's method, FEA, Optimization.

*Corresponding author
Peer review under the responsibility of University of Baghdad.
https://doi.org/10.31026/j.eng.2024.04.04

Article received: 04/05/2023
Article accepted: 16/07/2023
Article published: 01/04/2024

أمثلية ومحاكاة لحام المقاومة النقطي للالمنيوم التجاري AA1050 باستخدام ماكنة لحام منخفضة القدرة

صافي رمزي صافي[1]،*، منير حميد طليفح[2]، محسن جبر جويج[3]

[1]قسم الهندسة الميكانيكية، كلية الهندسة، جامعة بغداد، بغداد، العراق

[2]جامعة بغداد، بغداد، العراق

[3]جامعة الفراهيدي، بغداد، العراق

الخلاصة

تهدف هذه الدراسة إلى إيجاد أفضل عوامل لحام المقاومة النقطي في الألومنيوم التجاري AA1050 للحصول على أقصى مقاومة شد للمفصل باستخدام آلة لحام ذات مصدر طاقة منخفض. المتغيرات المختارة لهذه الدراسة هي تيار اللحام ووقت اللحام وقوة القطب باستخدام ماكنة لحام ذات قدرة 90 kVA. تم استخدام طريقة DoE (تصميم التجارب) مع تقنية تاكوجي لتقليل عدد التجارب حيث تم استخدام صفيحتين بسمكين (1 ملم و 2 ملم) في هذا العمل. حللت النتائج بواسطة برنامج Minitab 18 باستخدام مخطط المؤثرات الرئيسية ومخطط التفاعل لتحديد العوامل الاكثر اهمية وتأثيرها على قوة المفصل. أفضل العوامل التي تم الحصول عليها لأعلى قوة شد قصي كانت 14.85 كيلو أمبير لتيار اللحام و 0.79 كيلو نيوتن لقوة القطب لكلا السمكين ودورتين و 12 دورة لحام لسمك الصفيحة 1 ملم و 2 ملم ، على التوالي. كانت أقصى مقاومة شد تم الحصول عليها هي 250 نيوتن و 225 نيوتن لسمك 1 ملم و 2 ملم على التوالي. وضعت معادلة رياضية للتنبؤ بقوة الشد القصي بنسبة خطأ 19.9 % و 17.9% لكل من الصفيحتين 1 ملم و 2 ملم ، على التوالي. أفضل العوامل طبقت في ANSYS 2022R1 للحصول على توزيع درجة الحرارة مع التاريخ الزمني حيث تظهر النتيجة حجم الكتلة الصلبة وفقًا لدرجة حرارة الانصهار. ان نسبة الفرق بين الحجم الحقيقي والرقمي للكتلة الصلبة كان 8 %.

الكلمات المفتاحية: لحام المقاومة النقطي ، الألومنيوم التجاري AA1050 ، طريقة تاكوجي ، FEA ، الامثلية.

1. INTRODUCTION

The Aluminium alloy used is growing in the industry, especially in the body structure of the automotive industry **(Qiu et al., 2011)**. Its unique properties, e.g., the weight-to-strength ratio, make Aluminium a good choice for replacing heavy material like carbon steel **(Kim and Wallington, 2016)** to provide high strength at a lightweight.

Commercial Aluminium, located in the first series of aluminium alloys, is the weakest alloy compared to the other series of Aluminium. According to the other valuable properties, considerable attention was received on AA1050 in many industries **(Mabuwa and Msomi, 2020; Albaijan et al., 2022)**.

The type of welding used for joining sheets is resistance spot welding, the dominant process used in the automotive industry **(Ertas et al., 2009)** due to its high productivity and flexibility with low cost. Resistance spot welding (RSW) exploits the Joule heat law that generates in the metal by passing electrical current due to the electrical resistance.

According to the high electrical conductivity of Aluminium, there are challenging to use RSW in Aluminium. The researchers do a lot of work to obtain a good understanding of the effect of the parameters on the resistance spot welding in Aluminium, focusing on the AA5xxx and

AA6xxx series, where **(Hao et al., 1996)** developed prediction equations for different current types to welding AA5754 sheets and **(Ji and Zhou, 2004)** study the behavior of the electrode force and displacement during the resistance spot welding process for welding AA5182 sheets. Also, **(Florea et al., 2012)** study the effect of the welding current on the fatigue life of RSW joint in AA6061 sheets. The literature lacking the investigation of RSW in AA1050 makes a few researchers deal with it.

(Darwish and Al-Dekhial, 1999) characterize the parameters of RSW in AA1050, concluding the sheet thickness, which negatively affects the response equation developed to predict the fracture load. The RSW is a complicated process affected by several factors at different levels where the welding current, welding time, and electrode force are the most significant parameters **(Cho et al., 2006)** that predict the welding result is complex and then reduce the parameters produce a more predictable result **(Hussein and Barrak, 2016)**. On another side, researchers try to improve the strength of the spot welding joint by different approaches, e.g., using cover plates of steel to increase the resistance between the electrodes due to increasing temperature **(Satonaka et al., 2006; Qiu, Iwamoto and Satonaka, 2009)**, and using an additive powder to the faying surface to enhance the metallurgical properties of the RSW joint **(Al-Saadi and Hussein, 2013; Al Naimi et al., 2015)**.

Taguchi's method was used early to optimize spot welding parameters for steel **(Raut and Achwal, 2014; Dhawale and Name, 2019)** and Aluminium **(Hussein and Barrak, 2016)** to find out the maximum tensile shear strength of the joint. **(Hussein and Barrak, 2016)** utilized Minitab program software to allocate the parameters and analyze the response data using mean effect and interaction plots.

To simulate the welding process, three software programs provide a numerical solution for the RSW process: SORPAS, Simufact, and ANSYS multi-physics. The RSW for Aluminium was not found in the literature; on the contrary, several researchers have applied welding conditions of Aluminium alloys in SORPAS software to develop a numerical Aluminium alloy model **(Kim et al., 2019; Lee, 2020; Schulz et al., 2021)**.

In the current study, Taguchi's method was used to optimize the parameters of RSW for AA1050 sheets depending on the main welding parameters; welding current, welding time, and electrode force. Also, ANSYS multi-physics was chosen to develop a numerical model of AA1050. The best conditions of RSW, obtained from the optimization, will be applied in the ANSYS to investigate the temperature distribution with time history.

2. TAGUCHI METHOD

It is a statistical method based on the orthogonal array methods used widely in the engineering experiments design. This technique provides an efficient and powerful method for designing processes with various conditions. As mentioned previously, the properties of the DoE Taguchi method reduce the number of experiments and then reduce the cost of the total experiments. Taguchi used the signal-to-ratio (S/N) ratio for the quality characteristic, a measurable value that replaced the standard deviation. It was used to design the experiments and analyze the results to achieve the best conditions of the resistance spot welding in commercial Aluminium. This method is provided by program software Minitab, which solves all the mathematical procedures of Taguchi's method depending on the input data.

3. EXPERIMENTAL WORK

3.1 Materials and Welding Machine

The experiments are performed using commercial Aluminium AA1050 sheets with 1 mm and 2 mm thicknesses since commercial Aluminium lacks in literature and its unique properties, e.g., corrosion resistance and decent appearance. In addition, the weakness of this alloy and its weldments as compared to the other alloys of Aluminium makes the limitation of choosing it as a structural material. The Aluminium's mechanical properties and chemical composition are shown in **Table 1 and Table *2***. Both the chemical and mechanical analysis were done by the Engineering Insp. & lab Department/SIER/Ministry of Industry and Minerals/the Republic of Iraq. The AA1050 sheets were cut into strips with the dimensions shown in **Figure 1** according to the American Welding Society **(AWS B 4.0, 2016),** and the longitudinal cuts were parallel to the rolling direction. All the strips of the same thickness are cut from the same sheet to ensure the mechanical properties and chemical composition match.

Table 1. Mechanical Properties of commercial Aluminium AA1050 sheet

Sample	Ultimate stress (N/mm^2)	Yield stress ($N/mm^{2)}$	Elongation (%)	Hardness (HV)
1mm	99.72	96.74	7	34
2mm	126.38	114.84	9	44

Table 2. Chemical composition of commercial Aluminium AA1050 sheet

Sample	Si%	Fe%	Cu%	Mn%	Mg%	Cr%	Ni%	Zn%	Ti%	Al%
1mm	0.0641	0.366	0.0185	0.0062	0.001	0.0014	0.0011	0.0089	0.0147	99.5
2mm	0.0473	0.292	0.0172	0.002	0.0014	0.0019	0.003	0.001	0.0192	99.6

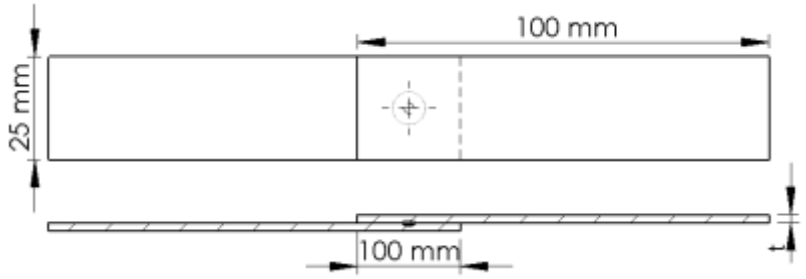

Figure 1. Schematic of the strip configuration for RSW

All the welds were achieved in Technical Engineering Collage/Baghdad using the SIP Column PPV50 machine with the specifications in **Table 3**.

Table 3. Specifications of RSW machine SIP Column PPV50

Specification	Controller	Current type	Max. welding power	Supply voltage	Frequency	Max. electrode force	Electrode force per 1 bar
Value	CSW-02 7 function	AC	90 kVA	380 V	50 Hz	3.14 kN	0.785 kN

The electrodes used for welding have coned-shaped male caps with copper-chromium (C18200) composition (RWMA group A, class 2 alloy) and the trade name Miller A-2508 Pointed Nose Tip. The contact diameter was 8 mm with a flat end surface.

3.2 Methodology

The main parameters affected by RSW are welding current, welding time, and electrode force **(Cho et al., 2006)**. Therefore, these parameters are chosen for the DoE with five levels for the tensile shear strength test for each thickness. **Table 4** shows the parameters with the values at each level.
The orthogonal array can be selected depending on the factors' number and the levels. The tests used an L25 orthogonal array with three factors and five levels, as shown in **Table 5**.

Table 4. Parameters values at different levels

Thickness	Process parameter	Unit	Level 1	Level 2	Level 3	Level 4	Level 5
1 and 2 mm	Welding current	kA	14.85	14.25	13.5	12	10.5
	weld time	Cycle	2	4	8	10	12
	Electrode force	kN	0.7854	1.37	1.96	2.55	3.14

Table 5. Experimental layout using L25 orthogonal array

Exp. No.	Welding current (kA)	Welding time (cycle)	Electrode force (kN)	Exp. No.	Welding current (kA)	Welding time (cycle)	Electrode force (kN)
1	14.85	2	0.785	14	13.5	10	0.785
2	14.85	4	1.37	15	13.5	12	1.37
3	14.85	8	1.96	16	12	2	2.55
4	14.85	10	2.55	17	12	4	3.14
5	14.85	12	3.14	18	12	8	0.785
6	14.25	2	1.37	19	12	10	1.37
7	14.25	4	1.96	20	12	12	1.96
8	14.25	8	2.55	21	10.5	2	3.14
9	14.25	10	3.14	22	10.5	4	0.785
10	14.25	12	0.785	23	10.5	8	1.37
11	13.5	2	1.96	24	10.5	10	1.96
12	13.5	4	2.55	25	10.5	12	2.55
13	13.5	8	3.14				

3.3 Tensile Shear Strength Test

A universal testing machine tested all the specimens of RSW in the strength of the material laboratory/Mechanical Engineering Department/College of Engineering/University of Baghdad. The tensile tests were performed at 2 mm/min load speed. The specimens were gripped with the shim on each side. The shim thickness is equal to the specimen's thickness that was grabbed to it to make sure a pure shear is obtained. The specimen with the shims can be shown in **Figure 2**.

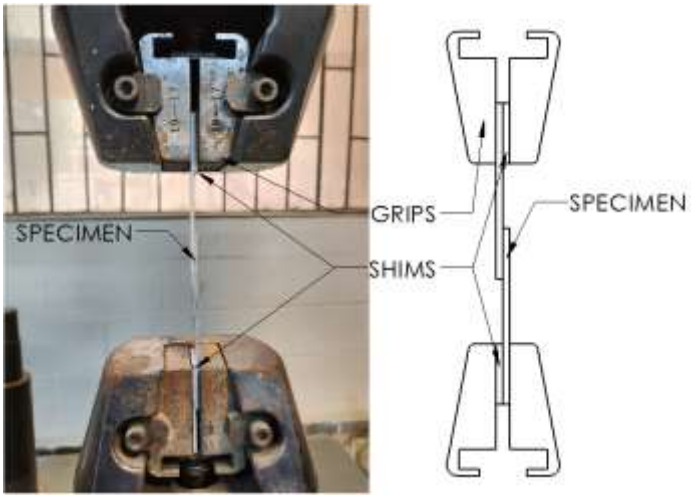

Figure 2. Illustration of the gripped specimen with shims

4. RESULTS AND DISCUSSION

4.1 Tensile Shear Strength

The experiment results of tensile shear strength for the RSW joint of the sheets with the two thicknesses (1 mm and 2 mm) are shown in **Figure 3**. The highest value of the joint strength was demonstrated in the 1 mm thickness sheet. The results show a contract because the number of levels chosen makes the level with a negative effect lead to poor strength.

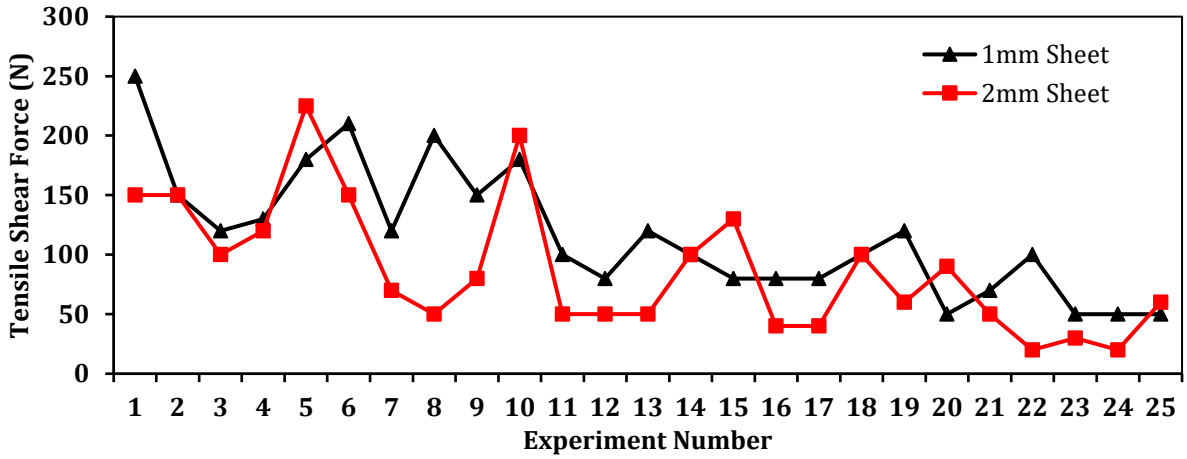

Figure 3. Tensile shear force results of RSW for 1 mm and 2 mm thicknesses.

4.2 DoE results

The software program Minitab 18 was used to analyze the shear force results. The input data are the same as the results shown in **Figure 3**.
The main effect plot (**Figure 4** and **Figure *5***) shows the effect of current on RSW strength. The increases in the current cause increasing joint strength because of the rise of heat generation due to the current surge, which leads to a bigger nugget size. **Table 6** shows the ANOVA results for the RSW parameters.

Table 6. Analysis of variance for RSW parameters

	Source	DF	Adj SS	Adj MS	F-value	P-value
1 mm sheet	Current	1	3.4328	3.43277	42.73	0.000
	Time	1	0.1386	0.13864	1.73	0.203
	Force	1	0.137	0.13701	1.71	0.206
	Error	21	1.687	0.08033		
	Total	24	5.3954			
2 mm sheet	Current	1	5.7185	5.7185	33.00	0.000
	Time	1	0.6804	0.6804	3.93	0.061
	Force	1	0.3863	0.3863	2.23	0.15
	Error	21	3.6387	0.1733		
	Total	24	10.4239			

The effect of welding time shows a difference between the RSW in 1 mm and 2 mm sheet thicknesses. The increasing welding time in 1 mm sheet thickness results in generating multi nuggets with small size, which means weaker joints, but in 2 mm sheet thickness, increasing welding time caused increasing nugget size.

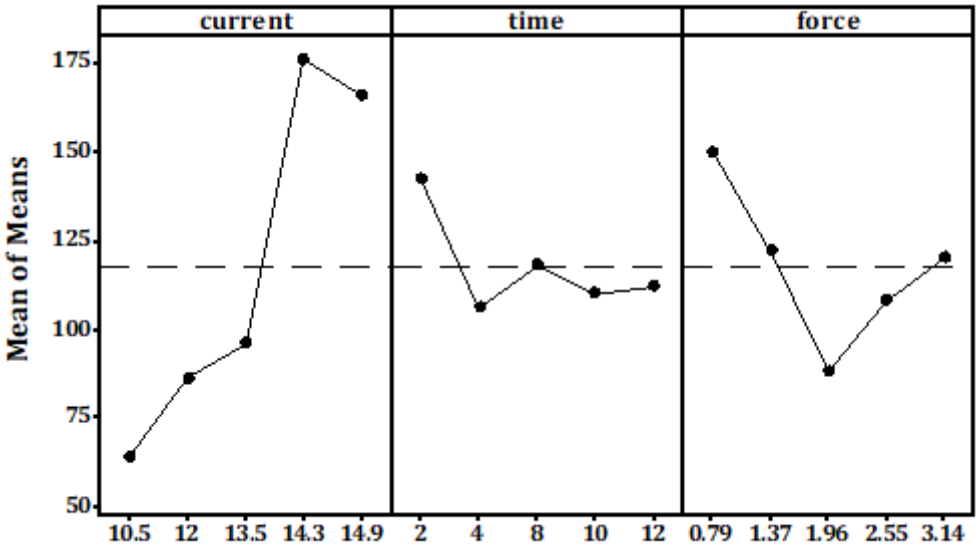

Figure 4. Main effects plot of shear strength for RSW of 1 mm sheet thickness

The electrode force with the range (0.79 kN - 1.96 kN) shows the same behavior in both thicknesses, in which the strength decreased with increasing electrode force. The electrode force increases the contact area, reducing current density and heat dissipation **(Cui et al., 2014; Hou et al., 2014)**. In addition, the electrode force breaks down the oxide layer, reducing the resistance contact **(Rashid et al., 2011)**. All these reasons caused a reduction in the nugget size and produced weaker joints.

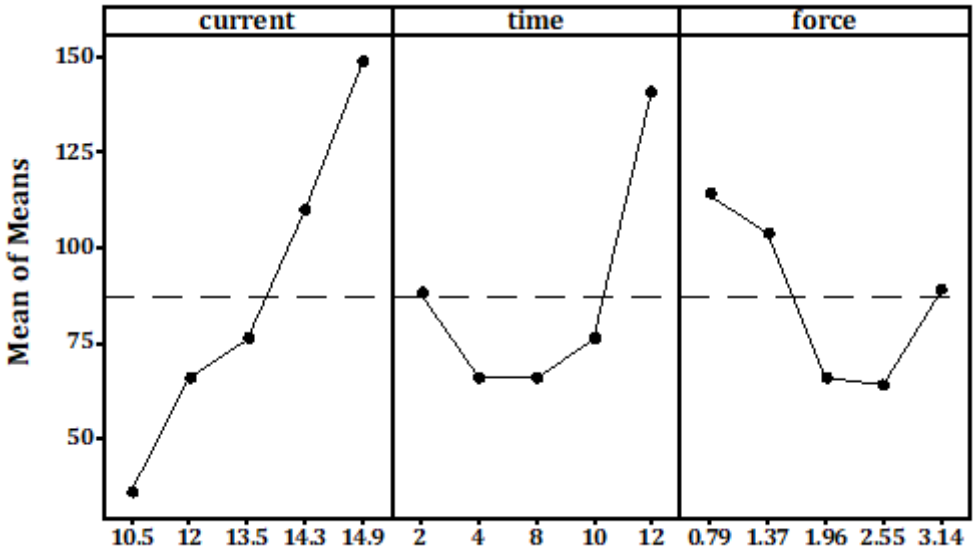

Figure 5. Main effects plot of shear strength for RSW of 2 mm sheet thickness

The interaction plots (**Figure 6** and **Figure 7**) show the effect of each parameter separately on the shear force. These plots support the discussion on the primary effects plots and add information on the impact of each level on the response, e.g., the current 10.5 kA has a negligible impact on the shear force in all conditions for both thicknesses. The high welding current produces a higher shear strength. But if the time effect is considered, a different response is achieved where increasing welding time at high welding current decreases the shear force for 1 mm sheet thickness at variance to 2 mm sheet thickness.

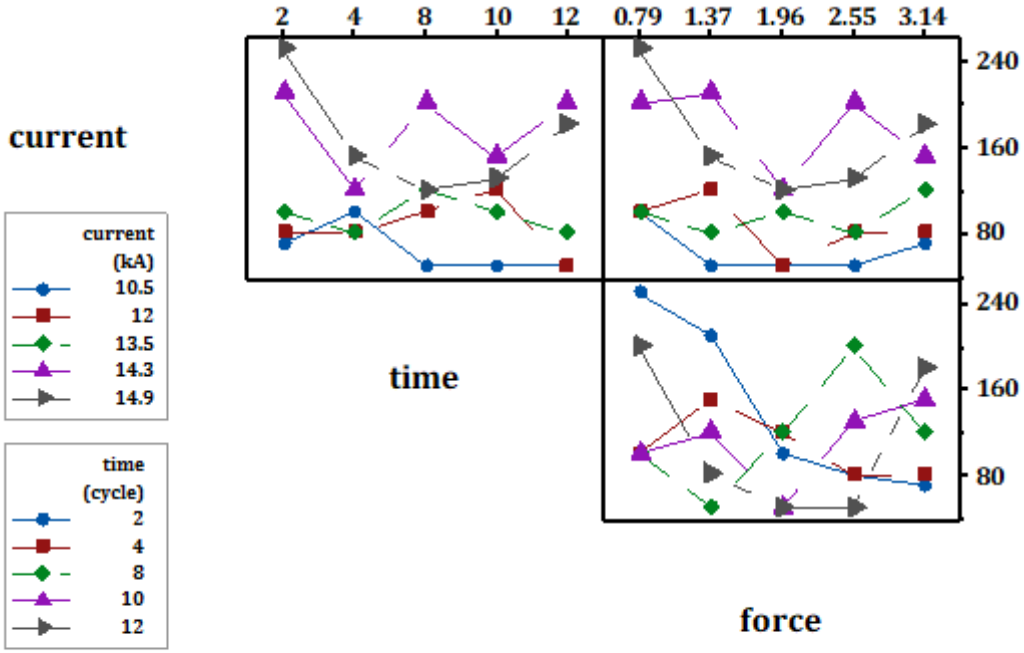

Figure 6. Interaction plot of shear force for 1 mm sheet thickness

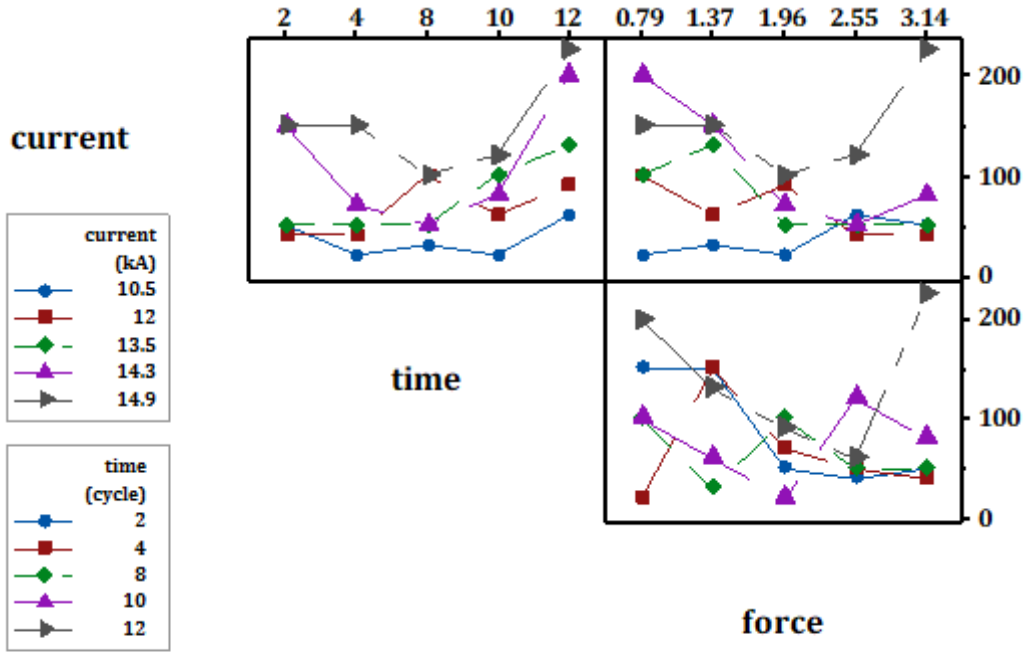

Figure 7. Interaction plot of shear force for 2 mm sheet thickness

4.3 The Response Equation

The software program (Minitab 18) gives a mathematical formula that represents the response (*shear force*) as a function of the parameters (welding current, welding time, and electrode force) depending on the DoE results. The exponential equations were chosen to describe the response results, as shown in **Eq. 1**.

$$Shear\ Force\ = \begin{cases} e^{1.927+0.2345I-0.0201t-0.0889F} & for\ 1mm\ thickness \\ e^{0.306+0.3027I+0.0445t-0.149F} & for\ 2mm\ thickness \end{cases} \quad (1)$$

where I is the welding current, t is the welding time, and F is the electrode force.
The best conditions parameters are specified by the Response Optimizer method provided in Minitab 18 according to the maximum tensile force the specimens failed at. The best conditions, mathematical and actual results, and the validation error can be listed in **Table 7**.

Table 7. Best RSW parameters, mathematical and actual results, and percentage of discrepancy for welding current of 14.85 kA, and electrode force of 0.79 kN

Thickness (mm)	Best welding time (cycle)	Mathematical results (N)	Actual results (N)	Discrepancy (%)
1	2	200.2	250	19.9
2	12	184.6	225	17.9

4.4 Numerical Simulation

The simulation uses coupled field elements called PLANE223 in ANSYS 2022R1, considering structural, thermal, electrical, and contact conditions. The geometric model is built according to the real dimensions and configuration. The model analyzing the distribution of temperature and stresses is similar to the work of **(Deng et al., 2020)**. All the governing equations of the coupled field element used for resistance spot welding are described briefly by **(Wan et al., 2016; Zhao et al., 2019; Huang et al., 2020)**. The temperature dependence properties input in ANSYS material for AA1050 and the electrode received from the literature are shown in **Table 8**.
The contact resistance between the electrode and the sheet and between the two sheets is calculated using **(Zhao et al., 2019)**:

$$ECR_{(T,P)} = 3d\left(\frac{\rho_{1(T)}+\rho_{2(T)}}{2}\right)\left(\frac{\sigma_{ys(T)}}{P}\right)^{k} \quad (2)$$

where *ECR* is the electrical contact resistance, *T* is temperature, *P* is pressure contact MPa, *d* is the contact layer thickness, which varies from 0.01mm to 0.05mm **(Wan et al., 2016)**, ρ_1 and ρ_2 specific resistance for the electrode and the Aluminium, respectively, and σ_{ys} is the yield strength for Aluminium. The *k* is an additional factor that varies between 1 and 1.5. All the factors applied in this equation are listed in **Table 8**. **Figure 8** gives the welding parameters used to simulate 2 mm sheet thickness, where the electrode force is 785 N, the welding time is 0.24 sec, and 14.85 kA for welding time.

Table 8. The temperature-dependence properties of AA1050 and the electrode

Copper electrode (RWMA Class 2) **(Wang et al., 2015)**				AA1050 H14 **(Brandt and Neuer, 2007)**			
Temperature, °C	Thermal conductivity, W/m.°C	Resistance, Ω.m × 10^{-8}	Modulus of elasticity, GPa	Temperature, °C	Thermal conductivity, W/m.°C	Resistance, Ω.m × 10^{-8}	Yield strength (MPa) **(Shrivastava et al., 2018)**
21	390	2.6	124	25	268	2.71	113.8
93	380	3	105	100	250	3.64	…
204	370	4	93	200	234.6	4.92	70
316	355	5.1	82	300	225.9	6.19	40
427	345	6.2	55	400	225	7.3	…
538	334	7	38	500	219	8.61	10
649	320	8	25	600	217	9.88	…
760	316	9	…	650	212.5	10.64	…

The simulation of the RSW process of the Aluminium is shown in

Figure 9, where the red zone represents the fusion zone and nugget size. The actual nugget diameter at the same conditions measured from the fractured sample was 2.5 mm, whereas the simulation shows 2.3 mm. The disparity between actual and simulation results might be due to the contact properties not matching the real conditions where the contact resistance

is affected by oxide thickness, contamination of the surface, and roughness. The time history of the temperature in the center of the nugget is shown in **Figure 10**.

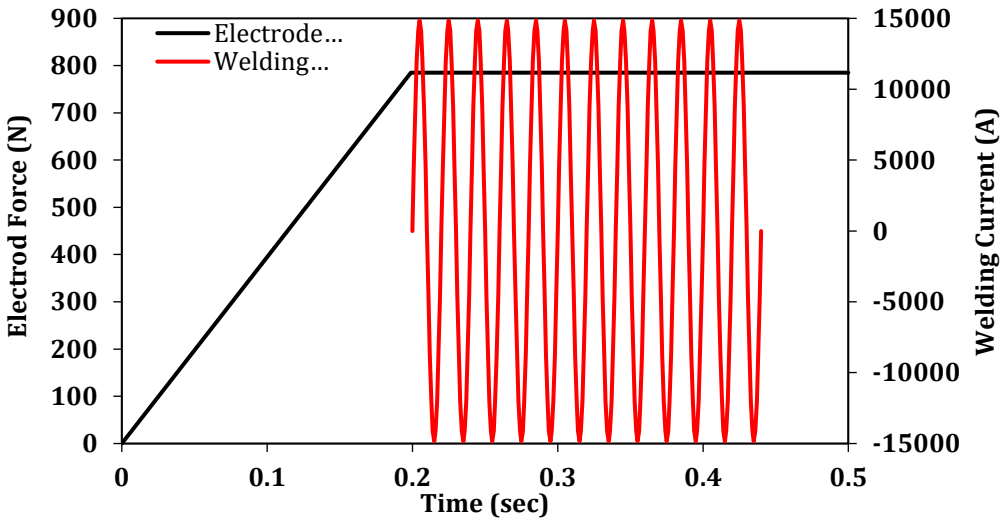

Figure 8. Welding parameters for the RSW simulation process

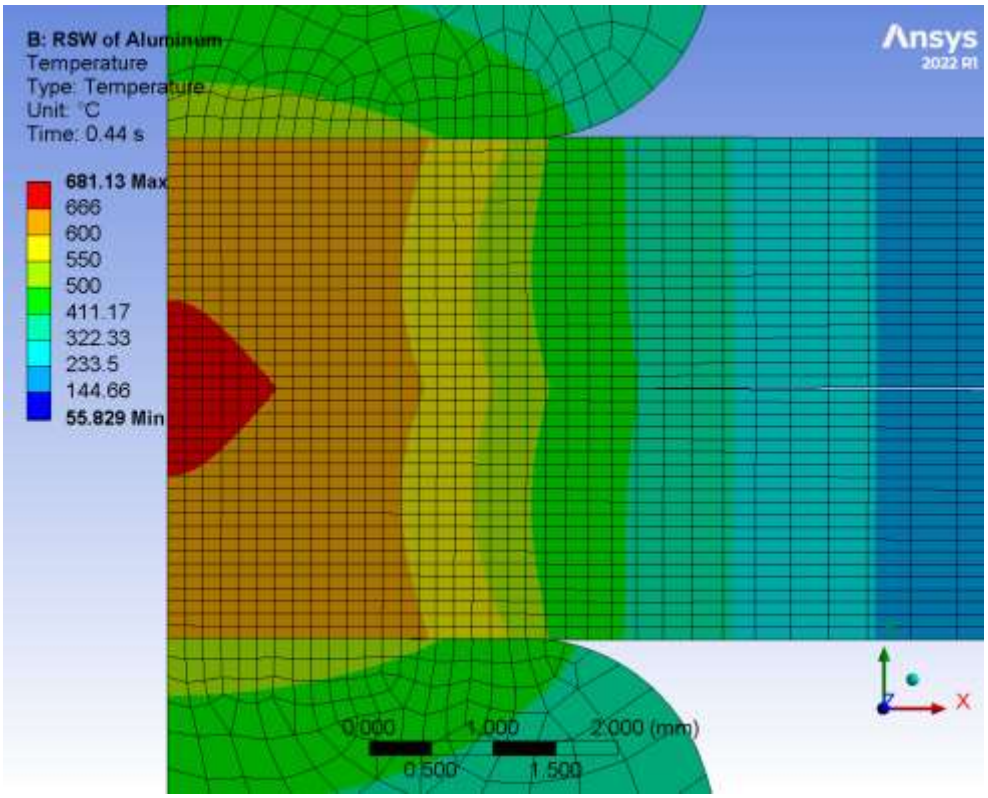

Figure 9. Temperature distribution of the welding zone after 12 cycles of the welding time

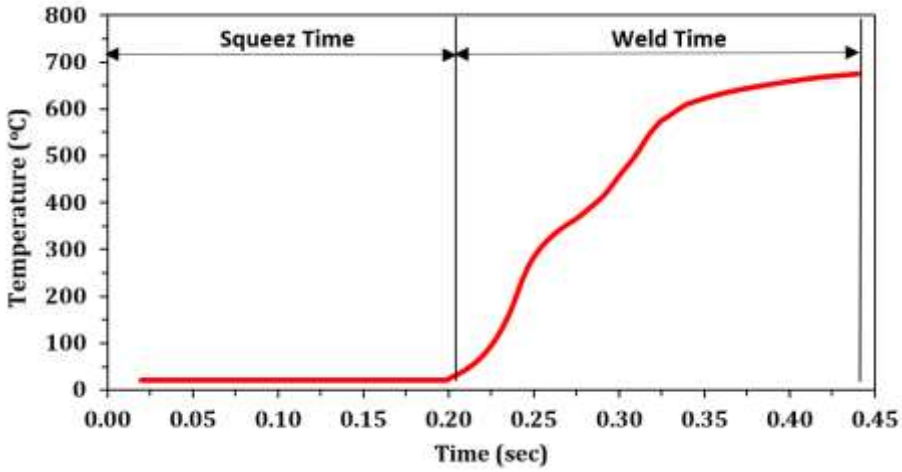

Figure 10. The time history in the center of the nugget during the welding process

5. CONCLUSIONS

Taguchi method is used to design experiments to reduce the number of experiments from 225 (in the whole factorial process) to 25 experiments to find significant parameters of RSW and their values to produce maximum tensile strength using a low-power welding machine. The conclusions of the current study are summarized as follows:

1. The effect of parameters on the shear force was obtained by analyzing mean effects plots and interaction plots. The welding current shows the most significant impact on the RSW process.
2. Regardless of the sheet thickness, increasing the welding current increases the strength of the joint. Otherwise, increasing welding time decreased RSW joint strength for the 1 mm sheet thickness and improved it for the 2 mm sheet thickness. The electrode force shows a negative effect on the strength.
3. The maximum shear force for the 1 mm sheet thickness was obtained at 14.85 kA welding current, 2-cycle welding time, and 0.79 kN electrode force. Similarly, for the 2 mm sheet thickness, the maximum shear force was obtained at 14.85 kA welding current, 12-cycle welding time, and 0.79 kN electrode force.
4. Prediction equations were established for both thicknesses, showing a discrepancy of 19.9% for the 1 mm sheet thickness and 17.9% for the 2 mm sheet thickness.
5. A numerical model is developed to study the temperature distribution with time history at different conditions.

NOMENCLATURE

Symbol	Description	Symbol	Description
d	Contact layer thickness, mm	P	Pressure contact, MPa
ECR	Electrical contact resistance, Ω	T	Temperature, °C
F	Electrode force, kN.	t	Welding time, cycle
I	Welding current, kA	ρ	Specific resistance Ω. m
k	Factor that varies between 1 and 1.5	σ_{ys}	Yield strength for aluminum

Acknowledgements

This work was supported by the College of Engineering, University of Baghdad. The authors gratefully acknowledge the PLS lab staff in the Department of Mechanical Engineering within the College of Engineering. Without their help and contribution, this work would not accomplished.

Credit Authorship Contribution Statement

Safi R. contributed primarily to the conception, design, and execution of the numerical simulations, as well as the analysis and interpretation of the data, writing. Prof. Dr. Moneer Hameed Toliphih provided significant support in refining the simulation methodology, data analysis, and manuscript drafting. Prof. Dr. Muhsin Jaber Jweeg donated expertise in validating the simulation results and provided critical insights during the manuscript preparation and editing.

Declaration of Competing Interest

The authors declare that they have no known competing financial interests or personal relationships that could have appeared to influence the work reported in this paper.

REFERENCES

Albaijan, I., Ahmed, M.M.Z., El-Sayed Seleman, M.M., Touileb, K., Habba, M.I.A., and Fouad, R.A., 2022. Optimization of bobbin tool friction stir processing parameters of AA1050 using response surface methodology. *Materials*, 15(19), P. 6886. Doi:10.3390/ma15196886

Al-Saadi, M.H., and Hussein, S.K., 2013. Improvement of the strength of spot welding joint for Aluminium plates using powders as additive. *Engineering and Technology Journal*, 31(13 Part (A) Engineering). Doi:10.30684/etj.31.13A.4

AWS B 4.0, 2016. Standard methods for mechanical testing of welds. Approved by American National Standards Institute. https://pubs.aws.org/p/2113/b40-2016-amd1-standard-methods-for-mechanical-testing-of-welds

Brandt, R., and Neuer, G., 2007. Electrical resistivity and thermal conductivity of pure Aluminium and Aluminium alloys up to and above the melting temperature. *International Journal of Thermophysics*, 28, pp. 1429–1446. Doi:10.1007/s10765-006-0144-0

Cho, Y., Li, W., and Hu, S.J., 2006. Design of experiment analysis and weld lobe estimation for Aluminium resistance spot welding. *Welding Journal*, 85(3), pp. 45–51.

Cui, L.H., Qiu, R.F., Shi, H.X., and Zhu, Y.M., 2014. Resistance spot welding between copper coated steel and Aluminium alloy. *Applied Mechanics and Materials*. Trans Tech Publ. pp. 19–22. Doi:10.4028/www.scientific.net/AMM.675-677.19

Darwish, S.M., and Al-Dekhial, S.D., 1999. Statistical models for spot welding of commercial aluminium sheets. *International Journal of Machine Tools and Manufacture*, 39(10), pp. 1589–1610. Doi:10.1016/S0890-6955(99)00010-3

Deng, L., Li, Y., Cai, W., Haselhuhn, A.S., and Carlson, B.E., 2020. Simulating thermoelectric effect and its impact on asymmetric weld nugget growth in Aluminium resistance spot welding. *Journal of Manufacturing Science and Engineering*, 142(9). Doi:10.1115/1.4047243

Dhawale, P.A., and Name, B.P.R., 2019. Prediction of weld strength by parametric optimization of resistance spot welding using Taguchi method. *AIP conference proceedings*. AIP Publishing LLC. P. 020087. Doi:10.1063/1.5141257

Ertas, A.H., Vardar, O., Sonmez, F.O., and Solim, Z., 2009. Measurement and assessment of fatigue life of spot-weld joints. *Journal of Engineering Materials and Technology,* 131(1), P. 011011 (11 pages). Doi:10.1115/1.3030941

Florea, R.S., Solanki, K.N., Bammann, D.J., Baird, J.C., Jordon, J.B., and Castanier, M.P., 2012. Resistance spot welding of 6061-T6 Aluminium: Failure loads and deformation. *Materials & Design*, 34, pp. 624–630. Doi:10.1016/j.matdes.2011.05.017

Hao, M., Osman, K.A., Boomer, D.R., and Newton, C.J., 1996. Developments in characterization of resistance spot welding of Aluminium. *Welding Journal-Including Welding Research Supplement*, 75(1), pp. 1–4.

Hou, L.L., Qiu, R.F., Shi, H.X., and Guo, J.Q., 2014. Properties of resistance spot welded joint between mild steel and Aluminium alloy with an interlayer of AlCu28. *Applied Mechanics and Materials*. Trans Tech Publ. pp. 15–18. Doi:10.4028/www.scientific.net/AMM.675-677.15

Huang, M., Zhang, Q., Qi, L., Deng, L., and Li, Y., 2020. Effect of external magnetic field on resistance spot welding of Aluminium alloy AA6061-T6. *Journal of Manufacturing Processes*, 50, pp. 456–466. Doi:10.1016/j.jmapro.2020.01.005

Hussein, S.K., and Barrak, O.S., 2016. Optimization the resistance spot welding parameters of austenitic stainless steel and Aluminium alloy using design of experiment method. *Engineering and Technology Journal*, 34(7), pp. 1383–1401. Doi:10.30684/etj.34.7A.11

Ji, C.T., and Zhou, Y., 2004. Dynamic electrode force and displacement in resistance spot welding of Aluminium. *Journal of Manufacturing Science Engineering*, 126(3), pp. 605–610. Doi:10.1115/1.1765140

Kim, G.C., Hwang, I., Kang, M., Kim, D., Park, H., and Kim, Y.M., 2019. Effect of welding time on resistance spot weldability of Aluminium 5052 alloy. *Metals and Materials International*, 25, pp. 207–218. Doi:10.1007/s12540-018-0179-3

Kim, H.C., and Wallington, T.J., 2016. Life cycle assessment of vehicle lightweighting: a physics-based model to estimate use-phase fuel consumption of electrified vehicles. *Environmental Science & Technology*, 50(20), pp. 11226–11233. Doi:10.1021/acs.est.6b02059

Lee, T., 2020. Resistance spot weldability of heat-treatable and non-heat-treatable dissimilar aluminium alloys. *Science and Technology of Welding and Joining*, 25(7), pp. 543–548. Doi:10.1080/13621718.2020.1761619

Mabuwa, S., and Msomi, V., 2020. The effect of friction stir processing on the friction stir welded AA1050-H14 and AA6082-T6 joints. *Materials Today: Proceedings*, 26, pp. 193–199. Doi:10.1016/j.matpr.2019.10.039

Al Naimi, I.K., Al-Saadi, M.H., Daws, K.M., and Bay, N., 2015. Improving resistance welding of Aluminium sheets by addition of metal powder. *Proceedings of the Institution of Mechanical Engineers, Part L: Journal of Materials: Design and Applications*, 229(6), pp. 493–502. Doi:10.1177/1464420714533526

Qiu, R., Iwamoto, C., and Satonaka, S., 2009. The influence of reaction layer on the strength of Aluminium/steel joint welded by resistance spot welding. *Materials Characterization*, 60(2), pp. 156–159. Doi:10.1016/j.matchar.2008.07.005

Qiu, R., Zhang, Z., Zhang, K., Shi, H., and Ding, G., 2011. Influence of welding parameters on the tensile shear strength of Aluminium alloy joint welded by resistance spot welding. *Journal of Materials Engineering and Performance*, 20, pp. 355–358. Doi:10.1007/s11665-010-9703-4

Rashid, M., Medley, J.B., and Zhou, Y., 2011. Nugget formation and growth during resistance spot welding of aluminium alloy 5182. *Canadian Metallurgical Quarterly*, 50(1), pp. 61–71. Doi:10.1179/000844311X552322

Raut, M., and Achwal, V., 2014. Optimization of spot welding process parameters for maximum tensile strength. *International Journal of Mechanical Engineering and Robotics Research*, 3(4), pp. 507–517.

Satonaka, S., Iwamoto, C., Qui, R., and Fujioka, T., 2006. Trends and new applications of spot welding for aluminium alloy sheets. *Welding international*, 20(11), pp. 858–864. Doi:10.1533/wint.2006.3677

Schulz, E., Wagner, M., Schubert, H., Zhang, W., Balasubramanian, B., and Brewer, L.N., 2021. Short-pulse resistance spot welding of Aluminium alloy 6016–T4—Part. *Welding Journal*, 100. Doi:10.29391/2021.100.004

Shrivastava, P., Kumar, P., Tandon, P., and Pesin, A., 2018. Improvement in formability and geometrical accuracy of incrementally formed AA1050 sheets by microstructure and texture reformation through preheating, and their FEA and experimental validation. *Journal of the Brazilian Society of Mechanical Sciences and Engineering*, 40, pp. 1–15. Doi:10.1007/s40430-018-1255-9

Wang, J., Wang, H.P., Lu, F., Carlson, B.E., and Sigler, D.R., 2015. Analysis of Al-steel resistance spot welding process by developing a fully coupled multi-physics simulation model. *International Journal of Heat and Mass Transfer*, 89, pp. 1061–1072. Doi:10.1016/j.ijheatmasstransfer.2015.05.086

Wan, Z., Wang, H.-P., Wang, M., Carlson, B.E., and Sigler, D.R., 2016. Numerical simulation of resistance spot welding of Al to zinc-coated steel with improved representation of contact interactions. *International Journal of Heat and Mass Transfer*, 101, pp. 749–763. Doi:10.1016/j.ijheatmasstransfer.2016.05.023

Zhao, D., Wang, Y., Zhang, P., and Liang, D., 2019. Modeling and experimental research on resistance spot welded joints for dual-phase steel. *Materials*, 12(7), P. 1108. Doi:10.3390/ma12071108